

TIGFlow-GRPO: Trajectory Forecasting via Interaction-Aware Flow Matching and Reward-Driven Optimization

Xuepeng Jing
xuepeng_j@tju.edu.cn
Tianjin University
Tianjin, China

Wenhuan Lu
Tianjin University
Tianjin, China

Hao Meng
Tianjin University
Tianjin, China

Zhizhi Yu*
Tianjin University
Tianjin, China

Jianguo Wei
Tianjin University
Tianjin, China

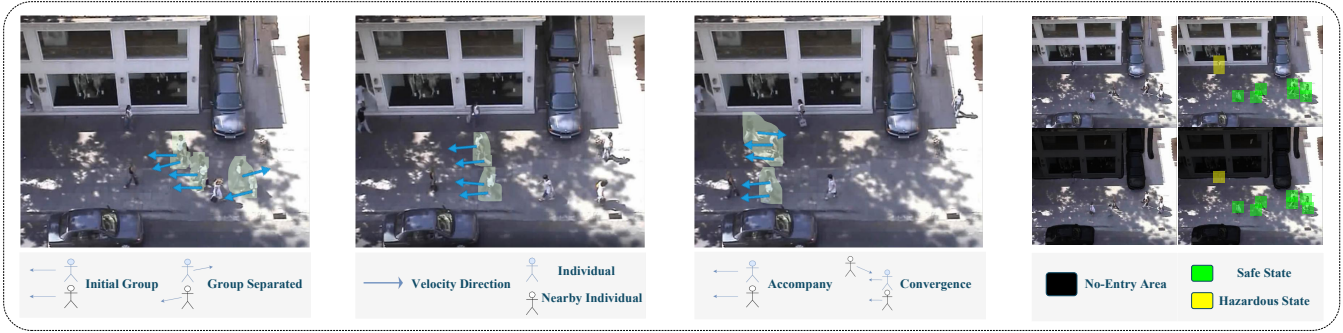


Figure 1: Representative examples of social interaction patterns and scene semantics. From left to right, the teaser shows group separation, individual motion direction, accompany and convergence behaviors, and semantic scene regions with different safety states, including no-entry, hazardous, and safe areas.

Abstract

Human trajectory forecasting is important for intelligent multimedia systems operating in visually complex environments, such as autonomous driving and crowd surveillance. Although Conditional Flow Matching (CFM) has shown strong ability in modeling trajectory distributions from spatio-temporal observations, existing approaches still focus primarily on supervised fitting, which may leave social norms and scene constraints insufficiently reflected in generated trajectories. To address this issue, we propose TIGFlow-GRPO, a two-stage generative framework that aligns flow-based trajectory generation with behavioral rules. In the first stage, we build a CFM-based predictor with a Trajectory-Interaction-Graph (TIG) module to model fine-grained visual-spatial interactions and strengthen context encoding. This stage captures both agent-agent and agent-scene relations more effectively, providing more informative conditional features for subsequent alignment. In the second stage, we perform Flow-GRPO post-training, where deterministic

flow rollout is reformulated as stochastic ODE-to-SDE sampling to enable trajectory exploration, and a composite reward combines view-aware social compliance with map-aware physical feasibility. By evaluating trajectories explored through SDE rollout, GRPO progressively steers multimodal predictions toward behaviorally plausible futures. Experiments on the ETH/UCY and SDD datasets show that TIGFlow-GRPO improves forecasting accuracy and long-horizon stability while generating trajectories that are more socially compliant and physically feasible. These results suggest that the proposed framework provides an effective way to connect flow-based trajectory modeling with behavior-aware alignment in dynamic multimedia environments.

CCS Concepts

• **Computing methodologies** → **Spatial and physical reasoning**; • **Human-centered computing** → *Interaction design theory, concepts and paradigms.*

Keywords

Trajectory Forecasting, Social Interaction Modeling, Flow Matching, Reinforcement Learning

Permission to make digital or hard copies of all or part of this work for personal or classroom use is granted without fee provided that copies are not made or distributed for profit or commercial advantage and that copies bear this notice and the full citation on the first page. Copyrights for components of this work owned by others than the author(s) must be honored. Abstracting with credit is permitted. To copy otherwise, or republish, to post on servers or to redistribute to lists, requires prior specific permission and/or a fee. Request permissions from permissions@acm.org.

Conference acronym '26, Woodstock, NY

© 2026 Copyright held by the owner/author(s). Publication rights licensed to ACM.
ACM ISBN 978-1-4503-XXXX-X/2018/06
<https://doi.org/XXXXXXXX.XXXXXXX>

ACM Reference Format:

Xuepeng Jing, Wenhuan Lu, Hao Meng, Zhizhi Yu, and Jianguo Wei. 2026. TIGFlow-GRPO: Trajectory Forecasting via Interaction-Aware Flow Matching and Reward-Driven Optimization. In *Proceedings of Make sure to enter the correct conference title from your rights confirmation email (Conference acronym '26)*. ACM, New York, NY, USA, 10 pages. <https://doi.org/XXXXXXX.XXXXXXX>

1 Introduction

Human trajectory forecasting is a fundamental problem in multimedia perception and spatio-temporal data mining [18, 28]. It supports applications such as autonomous driving, intelligent video surveillance, and human-robot interaction by providing predictive motion context. In dense and visually complex scenes, the task is to predict future pedestrian trajectories from observed motion histories while ensuring that the predicted paths are socially acceptable and physically feasible [17, 34]. This problem differs from conventional time-series forecasting because human motion is strongly influenced by uncertain intention, limited visual perception, nearby pedestrians, and surrounding scene geometry. Pedestrians continuously adjust their speed and direction in response to these factors, which makes future motion inherently multimodal [2, 16, 43]. Given the same observation history, several futures may be statistically plausible, although only some of them align well with real-world social norms and physical constraints.

A central challenge in trajectory forecasting is the gap between statistical distribution fitting and behavior-aware generation. Most recent methods are trained with supervised objectives, which encourage models to match empirical trajectory distributions [16, 43]. Although this strategy captures common motion patterns effectively, it does not directly optimize for compliance with environmental rules. As a result, incorporating non-differentiable physical constraints and social conventions into the training process remains difficult. When optimization criteria do not encode spatial boundaries or interaction logic, implausible behaviors may not be discouraged during generation [3, 13]. Small deviations introduced early in sequential prediction can then accumulate over time and move the rollout toward states that are poorly supported by the data. The resulting trajectories may remain statistically plausible while still violating basic constraints, for example by crossing obstacles or conflicting with nearby pedestrians [4, 18]. This mismatch suggests that reliable forecasting in interactive environments requires more than distribution fitting alone and motivates an explicit mechanism for behavioral alignment [8].

Recent progress in continuous-time generative modeling provides a useful foundation for this problem. Models such as diffusion models and CFM have shown strong performance in high-quality generation [6, 9, 20, 24]. In particular, CFM learns continuous normalizing flows through vector field regression, which yields stable training without simulation and supports efficient inference with few steps [24, 27]. Even so, applying CFM directly to trajectory forecasting does not resolve behavioral alignment, because the learning objective remains data-driven [13]. In parallel, RL has become an effective tool for aligning generative models with complex, non-differentiable preferences [11, 30, 37]. Among recent methods, Group Relative Policy Optimization (GRPO) is especially attractive

because it estimates relative advantages within a group of generated samples and therefore does not require a separate value network [35]. This design reduces memory overhead and simplifies policy updates, which makes GRPO well suited to generative modeling settings.

Bridging distribution fitting and behavioral alignment requires a framework that can optimize continuous generation under non-differentiable rules. Combining CFM with GRPO provides a practical route toward this goal. Standard CFM relies on deterministic rollout through an ordinary differential equation (ODE), which limits the trajectory exploration required by RL [24, 27]. To address this issue, we recast deterministic flow rollout during post-training as a stochastic differential equation (SDE) process, thereby injecting controlled stochasticity into generation [1, 7, 25, 36]. This reformulation creates an explorable policy space in which trajectories can be optimized with reward signals derived from the environment. On this basis, we use a stochastic flow policy as the optimization mechanism for behavior-aware alignment.

To realize this idea, we propose TIGFlow-GRPO, a forecasting framework that integrates CFM with online policy optimization. The model includes a TIG-GAT module that captures social context in a perception-aware manner. Rather than aggregating all nearby pedestrians indiscriminately, it selects neighbors according to the visual field of the target agent and refines the resulting interaction features for conditional generation, following the broader line of graph-based interaction modeling in trajectory forecasting [14, 34, 41, 42]. During post-training, we optimize the stochastic flow policy with a composite reward that evaluates each generated trajectory under visual-field-based social rules and signed distance field map constraints. This design encourages trajectories that remain compatible with both interpersonal behavior and scene geometry.

Our main contributions are summarized as follows.

- We introduce TIG-GAT, an interaction-aware perception module that improves social context modeling in crowded scenes through target-centric, view-aware neighbor reasoning and gated feature refinement. By combining perception-aware neighbor selection with explicit modeling of local interactions, TIG-GAT provides richer conditional representations for socially complex trajectory forecasting.
- During Flow-GRPO post-training, we reformulate deterministic flow rollout through an ODE-to-SDE transition, thereby turning continuous flow generation into a stochastic policy process. This design enables stochastic RL exploration and makes GRPO applicable to continuous spatio-temporal generation while preserving compatibility with the learned flow prior.
- We design a composite reward that integrates social and physical constraints, including view-aware interaction rules and scene-aware feasibility cues, to guide behavior-aware alignment during post-training. This reward encourages flow-based trajectory generation to produce futures that are more behaviorally plausible, socially consistent, and physically feasible.

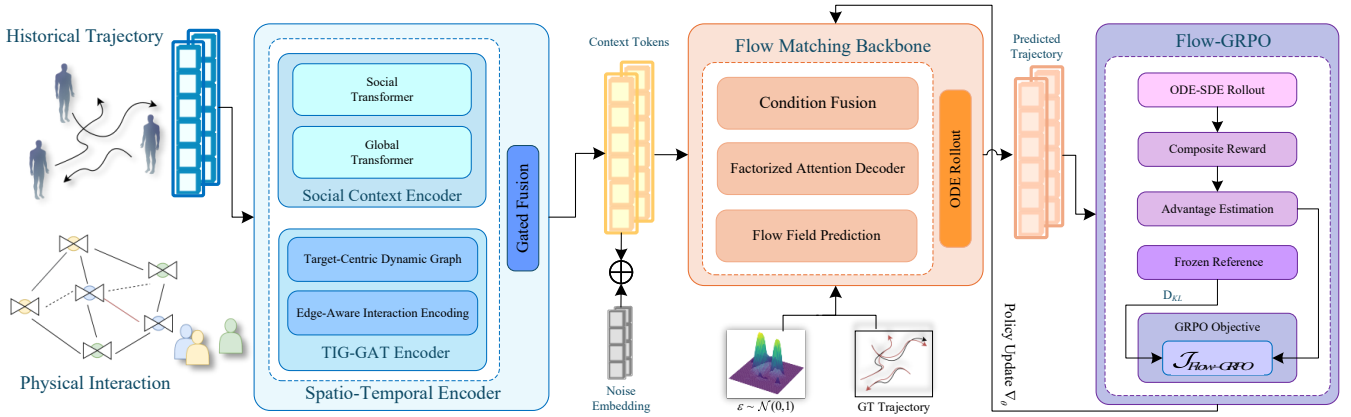


Figure 2: Overview of TIGFlow-GRPO. A spatio-temporal encoder produces context tokens from historical trajectories and interaction context, the flow-matching backbone generates future trajectories through ODE rollout, and Flow-GRPO post-training further aligns the predictions with social and physical constraints.

2 Related Work

2.1 Social Interaction Modeling in Crowds.

Early trajectory forecasting methods mainly relied on handcrafted motion priors and shallow sequential models, which offered only limited capacity to capture complex multi-agent interactions in crowded scenes. With the development of graph-based reasoning, methods such as Trajectron++ [34], GroupNet [41], EqMotion [42], and transferable GNN-based predictors [44] made interaction modeling a central component of trajectory forecasting. These methods represent pedestrians as nodes and model their relations through spatial proximity, relative motion, scene context, or group structure, thereby improving both local interaction reasoning and higher-order social dependency modeling. Recent studies further extend this direction by learning socially aware motion patterns [14] and interaction-aware stochastic formulations [12]. Even so, graph construction still involves a trade-off: dense connectivity may introduce noisy or redundant relations, whereas distance-based pruning may remove neighbors that are behaviorally informative. This challenge becomes more pronounced in visually complex scenes, where meaningful interaction cues depend not only on distance but also on perception, visibility, and local context. To better address this issue, TIG-GAT adopts target-centric, perception-aware neighbor selection and temporal gating, enabling the model to retain informative interactions while suppressing irrelevant social noise.

2.2 Generative Trajectory Forecasting.

Recent generative forecasting methods have increasingly focused on the intrinsic multimodality of human motion. Earlier latent-variable and structured-representation methods, such as SocialVAE [43] and EigenTrajectory [2], improve distribution modeling through time-dependent latent variables or low-rank motion descriptors. Diffusion-based predictors, including MID [16], SingularTrajectory [3], and DD-MDN [19], further enhance multimodal generation by formulating future prediction as a stochastic denoising process, while more recent distillation-based variants aim to

improve efficiency in multimodal forecasting [21]. By comparison, flow-based methods learn a continuous transformation from a simple prior to the target trajectory distribution, offering a favorable balance between training stability and sampling efficiency. MoFlow [13], in particular, demonstrates the potential of one-step flow matching for human trajectory forecasting. However, existing flow-based predictors for trajectory forecasting still depend mainly on supervised data fitting, and related flow-based generative models are also commonly trained with supervised objectives [9, 15, 32]. As a result, the alignment of generated trajectories with hard physical boundaries and complex social norms remains limited, which motivates our post-training alignment strategy for flow-based trajectory generation.

2.3 Policy Optimization and Constraints.

To handle non-differentiable real-world constraints, such as off-road penalties and scene-specific map compliance, RL provides a natural framework [30, 35, 37]. Recently, GRPO has emerged as an efficient critic-free policy optimization method and has attracted growing attention in LLM alignment and other generative settings [10, 35, 46]. Subsequent work has extended GRPO-style training to continuous generative models, showing that ODE-to-SDE conversion can introduce controllable stochasticity into otherwise deterministic flow rollouts [38, 45]. However, the use of this idea in human trajectory forecasting is still relatively limited. Unlike image or speech generation, motion forecasting must jointly account for multimodal diversity, positional accuracy, map-aware feasibility, and local collision avoidance. Motivated by this gap, TIGFlow-GRPO combines flow-based generation with GRPO and a tailored composite reward to better align the generative backbone with visual field rules and map constraints.

3 Methodology

3.1 Problem Formulation

Consider a visually complex crowd scene with A interacting agents. For a target agent $i \in \{1, \dots, A\}$, the observed trajectory over the

past T_h steps is denoted by $\mathbf{X}_i = \{\mathbf{x}_i^{-T_h+1}, \dots, \mathbf{x}_i^0\}$, where $\mathbf{x}_i^t \in \mathbb{R}^2$ is the 2D position at time step t . We define the conditioning context as $C_i = \{\mathbf{X}_i, \mathcal{N}_i, \mathcal{M}\}$, where \mathcal{N}_i encodes local social interactions under visual field rules and \mathcal{M} denotes scene topology. The goal is to model the conditional distribution of future motion $p(\mathbf{Y}_i | C_i)$, where $\mathbf{Y}_i = \{\mathbf{y}_i^1, \dots, \mathbf{y}_i^{T_f}\}$ is the future trajectory over the next T_f steps. To capture multimodal uncertainty, we adopt a Conditional Flow Matching (CFM) framework [13, 24], which learns a time-dependent vector field $v_\theta(\mathbf{z}_t, t, C_i)$ that transports a Gaussian prior $\mathbf{z}_0 \sim \mathcal{N}(\mathbf{0}, \mathbf{I})$ to the target distribution \mathbf{z}_1 through an Ordinary Differential Equation (ODE):

$$d\mathbf{z}_t = v_\theta(\mathbf{z}_t, t, C_i)dt, \quad t \in [0, 1]. \quad (1)$$

Since standard CFM relies on supervised fitting and does not explicitly enforce physical or social constraints, we further adopt a two-stage framework that combines flow-matching generation with ODE-to-SDE reformulation and reinforcement learning for behavioral alignment [10, 25, 36].

3.2 Overall Network Architecture

Figure 2 illustrates the two-stage TIGFlow-GRPO framework. During pretraining, a dual-branch Spatio-Temporal Encoder extracts conditional features from historical trajectories and interaction graphs. The implicit Social Context Encoder captures coarse crowd dependencies through social and global self-attention [39], whereas the TIG-GAT Encoder models target-centric local interactions via dynamic graph construction and edge-aware interaction encoding. Gated Fusion combines the two branches into context tokens that summarize global context and local interaction constraints. Conditioned on these tokens and a Gaussian noise embedding ($\epsilon \sim \mathcal{N}(\mathbf{0}, \mathbf{I})$), the Flow Matching Backbone predicts the flow field and performs ODE rollout to generate future trajectories [38]. At this stage, the model is trained with the standard flow-matching objective under future supervision.

During post-training, Flow-GRPO [25] reformulates the deterministic rollout as an ODE-to-SDE sampling process [1, 36]. The sampled trajectories are evaluated with a composite reward defined on the rollout and the scene conditions, converted into group-relative advantages [35], and optimized with a GRPO objective regularized by a frozen reference policy [25, 30]. The post-training objective depends only on sampled trajectories and scene context. The resulting policy update is fed back into the stochastic rollout, improving behavioral alignment while preserving multimodal diversity.

3.3 TIG-GAT Spatio-Temporal Feature Module

We use TIG-GAT to encode target-centric motion and local multi-agent interactions, while estimating the interaction complexity around the target agent.

Unlike conventional graph models built on dense social graphs [16, 18, 44], TIG-GAT adopts a target-centric dynamic graph. A cascaded Social Transformer [22, 39] first encodes the augmented historical states into an implicit social context $\mathbf{z}_i^{\text{soc}}$. For explicit interaction modeling, TIG-GAT then selects only the neighbors most relevant to the target agent. A field-of-view criterion defines the binary

visibility mask $m_{ij}^t = \mathbf{1}(\angle(\mathbf{v}_i^t, \Delta\mathbf{p}_{ij}^t) \leq \theta_{\text{FOV}})$, and the dynamic neighbor set $\tilde{\mathcal{N}}_i$ is constructed from accumulated visibility and spatial proximity over the historical window W :

$$\tilde{\mathcal{N}}_i = \text{TopK}_{j \in \mathcal{A} \setminus \{i\}} \sum_{\tau=-W+1}^0 m_{ij}^\tau \cdot \phi_{\text{sel}}(\|\Delta\mathbf{p}_{ij}^\tau\|_2). \quad (2)$$

Based on $\tilde{\mathcal{N}}_i$, we build a local interaction graph and introduce an Edge-Aware Gated Attention mechanism to alleviate the signal dilution of Softmax-based attention. Each edge is parameterized by relative kinematic features $\mathbf{e}_{ij}^t = \text{MLP}_{\text{edge}}([\Delta\mathbf{p}_{ij}^t \parallel \Delta\mathbf{v}_{ij}^t \parallel \|\Delta\mathbf{p}_{ij}^t\|_2 \parallel \cos \theta_{ij}^t])$. Message passing uses independent spatial gates:

$$\begin{aligned} \mathbf{g}_{ij}^t &= \sigma(\text{MLP}_{\text{spa}}([\mathbf{h}_i^t \parallel \mathbf{h}_j^t \parallel \mathbf{e}_{ij}^t])), \\ \mathbf{m}_i^t &= \sum_{j \in \tilde{\mathcal{N}}_i} \mathbf{g}_{ij}^t \odot (\mathbf{W}_V \mathbf{h}_j^t + \mathbf{W}_E \mathbf{e}_{ij}^t), \end{aligned} \quad (3)$$

where $\sigma(\cdot)$ denotes the Sigmoid activation function. This mechanism allows multiple relevant neighbors to contribute without competing through a normalized attention distribution [40].

After spatial aggregation, Temporal Gated Pooling summarizes the frame-wise physical features into a compact physical representation $\mathbf{h}_i^{\text{phy}}$, while the accumulated spatial gate activations provide a scalar interaction-strength estimate s_i . Finally, a strength-modulated gated residual fuses $\mathbf{h}_i^{\text{phy}}$ with the implicit context $\mathbf{z}_i^{\text{soc}}$ to produce the context token \mathbf{c}_i :

$$\begin{aligned} \mathbf{g}_i &= \sigma(\text{MLP}_{\text{fuse}}([\mathbf{z}_i^{\text{soc}} \parallel \mathbf{h}_i^{\text{phy}} \parallel s_i])), \\ \mathbf{c}_i &= \mathbf{z}_i^{\text{soc}} + \lambda s_i \mathbf{g}_i \odot \tanh(\mathbf{W}_{\text{phy}} \text{LN}(\mathbf{h}_i^{\text{phy}})). \end{aligned} \quad (4)$$

By combining implicit social context with explicit local interaction modeling, TIG-GAT produces the context representation used in the subsequent generative stages.

3.4 Flow-GRPO Post-Training

After supervised pretraining, we use Flow-GRPO as a post-training stage for trajectory forecasting [25]. Standard flow rollout is deterministic under a fixed scene condition [24, 27] and therefore does not provide the exploration needed to compare multiple plausible futures. We therefore preserve the pretrained flow prior and introduce stochasticity only during post-training, allowing the model to sample several candidate futures from the same observation and optimize them with trajectory-level rewards [10]. In our implementation, we use all rollout steps during optimization.

Let $v_\theta(\mathbf{y}_t, t, \mathbf{c}_i)$ denote the pretrained velocity field for latent state \mathbf{y}_t at time t under scene context \mathbf{c}_i . We keep the same Gaussian OT-CFM path as in pretraining, $\mathbf{y}_t = t\mathbf{y}_1 + (1-t)\xi$ with $\xi \sim \mathcal{N}(\mathbf{0}, \mathbf{I})$, so that post-training remains consistent with the learned flow prior. Under this Gaussian path, the score can be recovered directly from the velocity field [1, 30]. To avoid numerical instability near the endpoints, we use $\bar{t} = \text{clip}(t, \tau_{\min}, 1 - \tau_{\min})$. The recovered score and diffusion coefficient are

$$\begin{aligned} \mathbf{s}_\theta(\mathbf{y}_t, \bar{t}, \mathbf{c}_i) &= \frac{\bar{t} v_\theta(\mathbf{y}_t, \bar{t}, \mathbf{c}_i) - \mathbf{y}_t}{1 - \bar{t}}, \\ g(\bar{t}) &= \eta \sqrt{\frac{1 - \bar{t}}{\bar{t}}}. \end{aligned} \quad (5)$$

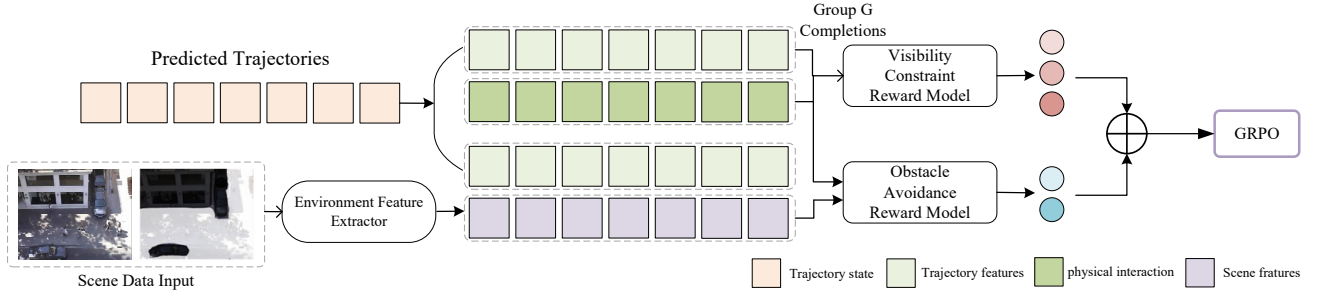


Figure 3: Flow-GRPO reward modeling and policy optimization. Predicted trajectories are organized into G completions and combined with environment features extracted from scene data. A visibility-constraint reward model and an obstacle-avoidance reward model evaluate each completion, and their outputs are aggregated for GRPO optimization.

Using the recovered score, we replace deterministic ODE rollout with the following stochastic transition [1, 25, 36]:

$$\begin{aligned} \mu_t &= \mathbf{y}_t + \left[v_\theta(\mathbf{y}_t, \bar{\mathbf{t}}, \mathbf{c}_i) + \frac{1}{2}g(\bar{\mathbf{t}})^2 s_\theta(\mathbf{y}_t, \bar{\mathbf{t}}, \mathbf{c}_i) \right] \Delta t, \\ \mathbf{y}_{t+\Delta t} &= \mu_t + \sigma_t \boldsymbol{\varepsilon}_t, \quad \sigma_t = g(\bar{\mathbf{t}}) \sqrt{\Delta t}, \quad \boldsymbol{\varepsilon}_t \sim \mathcal{N}(\mathbf{0}, \mathbf{I}). \end{aligned} \quad (6)$$

This transition defines a Gaussian policy at each rollout step and thus enables direct evaluation of stepwise log-probabilities [45]. Under the same scene condition, we sample G rollouts from a shared initial noise and evaluate each complete trajectory with the composite reward defined above.

For the g -th rollout, we compute the group-relative advantage $A_g = (\mathcal{R}_g - \mu_{\mathcal{R}}) / (\sigma_{\mathcal{R}} + \epsilon_{\text{adv}})$ [35, 38]. We further define the stepwise policy ratio $r_{g,t}(\theta) = \exp(\log p_\theta - \log p_{\text{old}})$ and its clipped version $\bar{r}_{g,t}(\theta) = \text{clip}(r_{g,t}(\theta), 1 - \epsilon_{\text{clip}}, 1 + \epsilon_{\text{clip}})$. To keep the updated policy close to the pretrained predictor, we introduce a frozen reference model and penalize the discrepancy between Gaussian transition means, which corresponds to the Gaussian KL term under a shared variance schedule [5]. The final objective is

$$\begin{aligned} \mathcal{L}_{\text{Flow-GRPO}} &= \frac{1}{G|S|} \sum_{g=1}^G \sum_{t \in S} \left[-\min(r_{g,t}(\theta) A_g, \bar{r}_{g,t}(\theta) A_g) \right. \\ &\quad \left. + \beta \frac{\|\mu_{\theta,g,t} - \mu_{\text{ref},g,t}\|_2^2}{2\sigma_t^2} \right]. \end{aligned} \quad (7)$$

This design makes Flow-GRPO a behavior-aware post-training method for trajectory forecasting, improving social and physical consistency while preserving the multimodal prior learned through supervised flow matching [25].

3.5 Reward Function Design

3.5.1 View-Aware Social Reward. To avoid treating all neighboring interactions equally, we define a view-aware social reward based on direction-sensitive geometry [14]. For the g -th predicted trajectory of target agent i , we first transform the prediction into the absolute coordinate system, $\hat{\mathbf{y}}_{i,g}^{t,\text{abs}} = \hat{\mathbf{y}}_{i,g}^t + \mathbf{x}_i^0$. We then construct frame-wise heading vectors from the sampled motion:

$$\mathbf{h}_{i,g}^t = \begin{cases} \hat{\mathbf{y}}_{i,g}^{1,\text{abs}} - \mathbf{x}_i^0, & t = 1, \\ \hat{\mathbf{y}}_{i,g}^{t,\text{abs}} - \hat{\mathbf{y}}_{i,g}^{t-1,\text{abs}}, & t > 1. \end{cases} \quad (8)$$

Based on the local heading, we identify relevant neighbors. Let $\mathbf{r}_{ij,g}^t = \hat{\mathbf{y}}_{j,g}^{t,\text{abs}} - \hat{\mathbf{y}}_{i,g}^{t,\text{abs}}$ denote the relative position vector [3]. The viewing angle $\theta_{ij,g}^t$ is computed only for neighbors within an interaction radius R and with valid heading support ($\|\mathbf{h}_{i,g}^t\|_2 > \epsilon$):

$$\theta_{ij,g}^t = \arccos \left(\frac{\langle \mathbf{h}_{i,g}^t, \mathbf{r}_{ij,g}^t \rangle}{\|\mathbf{h}_{i,g}^t\|_2 \|\mathbf{r}_{ij,g}^t\|_2 + \epsilon} \right). \quad (9)$$

We divide interactions into strong-view (s), weak-view (w), and rear-view (r) regions. Let $m_{ij,g}^t = \mathbf{1}(\|\mathbf{r}_{ij,g}^t\|_2 \leq R \wedge \|\mathbf{h}_{i,g}^t\|_2 > \epsilon)$ denote the valid-neighbor mask. The regional masks are defined by angular thresholds (ϕ_s, ϕ_w) :

$$\begin{aligned} \mathcal{M}_{ij,g}^{s,t} &= m_{ij,g}^t \cdot \mathbf{1}(\theta_{ij,g}^t \leq \phi_s), \\ \mathcal{M}_{ij,g}^{w,t} &= m_{ij,g}^t \cdot \mathbf{1}(\phi_s < \theta_{ij,g}^t \leq \phi_w), \\ \mathcal{M}_{ij,g}^{r,t} &= m_{ij,g}^t \cdot \mathbf{1}(\theta_{ij,g}^t > \phi_w). \end{aligned} \quad (10)$$

Using the predicted pairwise distance $\hat{d}_{ij,g}^t = \|\mathbf{r}_{ij,g}^t\|_2$ and its temporal change $\Delta \hat{d}_{ij,g}^t = \hat{d}_{ij,g}^t - \hat{d}_{ij,g}^{t-1}$, with $\hat{d}_{ij,g}^0 = \|\mathbf{x}_j^0 - \mathbf{x}_i^0\|_2$, we assign region-specific penalties. The strong-view region penalizes unsafe proximity, the weak-view region balances close contact and over-avoidance [25, 38] and the rear-view region only mildly penalizes excessive separation. With a scene-density normalization factor γ_i , the resulting reward is

$$\begin{aligned} r_{i,g}^{\text{sv}} &= -\gamma_i \text{Avg}_{j,t} \left(w_s \mathcal{M}_{ij,g}^{s,t} [\delta_s - \hat{d}_{ij,g}^t]_+^2 \right. \\ &\quad \left. + w_w \mathcal{M}_{ij,g}^{w,t} [\delta_w - \hat{d}_{ij,g}^t]_+^2 \right. \\ &\quad \left. + w_{wo} \mathcal{M}_{ij,g}^{w,t} [\Delta \hat{d}_{ij,g}^t - m_w]_+^2 \right. \\ &\quad \left. + w_r \mathcal{M}_{ij,g}^{r,t} [\Delta \hat{d}_{ij,g}^t - m_r]_+^2 \right). \end{aligned} \quad (11)$$

This reward introduces an explicit direction-sensitive social constraint into Flow-GRPO.

3.5.2 Map-Aware Semantic Reward and Fusion. For scenes with semantic maps, behaviorally plausible trajectories should also respect the static structure of the environment [14, 34]. We therefore define a map-aware semantic reward that incorporates walkable-area and obstacle priors into the reinforcement learning pipeline, complementing dynamic interaction constraints without modifying the flow backbone.

Table 1: Quantitative comparison of best-of- K ADE_{\min} / FDE_{\min} on the ETH/UCY benchmark, where the minimum error is reported over K predicted trajectories. Bold and underlined entries denote the best and second-best results, respectively. Lower values indicate better forecasting accuracy, and TIGFlow-GRPO achieves the best overall performance.

Dataset	GroupNet [41]	MID [16]	EqMotion [42]	EigenTraj [2]	LED* [29]	SingularTraj [3]	MoFlow [13]	DD-MDN [19]	TIGFlow-GRPO Ours
ETH	0.46/0.73	0.39/0.66	0.40/0.62	<u>0.37/0.54</u>	0.39/0.58	0.35/0.43	0.40/0.60	0.35/0.54	0.39/0.55
HOTEL	0.15/0.25	0.13/0.22	0.11/0.18	0.13/0.19	0.11/0.17	0.13/0.20	<u>0.12/0.18</u>	0.13/0.18	0.11/0.16
UNIV	0.26/0.49	0.22/0.45	<u>0.23/0.42</u>	0.24/0.40	0.26/0.44	0.26/0.45	<u>0.23/0.40</u>	0.24/0.42	0.22/0.38
ZARA1	0.21/0.39	<u>0.17/0.30</u>	0.18/0.34	0.19/0.33	0.18/ 0.26	0.19/0.33	<u>0.17/0.29</u>	<u>0.17/0.28</u>	0.16/0.26
ZARA2	0.17/0.33	<u>0.13/0.27</u>	<u>0.13/0.25</u>	0.14/0.24	<u>0.13/0.22</u>	0.15/0.26	<u>0.13/0.22</u>	0.12/0.21	0.12/0.21
AVG	0.25/0.44	<u>0.21/0.38</u>	0.22/0.36	0.21/0.34	<u>0.21/0.33</u>	0.22/0.33	<u>0.21/0.34</u>	0.20/0.32	0.20/0.31

For the g -th sampled future, we project the predicted trajectory in the absolute coordinate system onto the 2D map plane through the inverse rotation matrix R_i^{-1} of the focal agent and the scene homography H_i . To obtain continuous boundary feedback rather than discrete occupancy labels [3, 8], we precompute a Signed Distance Field (SDF), denoted by $S_i(\cdot)$, which returns the shortest clearance from a spatial point to the nearest obstacle boundary. The homogeneous projection and the resulting map-clearance evaluation are

$$\hat{d}_{i,g}^t = S_i \left(\Pi \left(H_i^{-1} \left[(R_i^{-1} \hat{\mathbf{y}}_{i,g}^{t, \text{abs}})^\top, 1 \right]^\top \right) \right), \quad (12)$$

where $\Pi(\cdot)$ denotes homogeneous coordinate normalization. For the observed history $\{\mathbf{x}_i^{k, \text{abs}}\}_{k \in O_i}$, we compute the corresponding clearances $d_i^{\text{obs}, k}$ through the same projection.

This formulation yields a continuous penalty for obstacle penetration and unsafe proximity to scene boundaries. To avoid over-penalizing trajectories that pass through narrow boundary-adjacent corridors, we adopt a relative-clearance formulation. We define the history-conditioned baseline map risk as $\hat{q}_i^{(\text{obs})} = \text{Avg}_{k \in O_i} [\delta_{\text{map}} - d_i^{\text{obs}, k}]_+^2$. The map-aware reward penalizes only the excess risk introduced by the prediction:

$$r_{i,g}^{\text{map}} = - \left[\text{Avg}_t [\delta_{\text{map}} - \hat{d}_{i,g}^t]_+^2 - \hat{q}_i^{(\text{obs})} \right]. \quad (13)$$

This reward encourages predicted trajectories to remain physically feasible with respect to the local scene geometry implied by the observed motion context [26].

Finally, we combine the map-aware reward, the view-aware social reward, and the regularizers for trajectory accuracy ($r_{i,g}^{\text{acc}}$) and motion smoothness ($r_{i,g}^{\text{sm}}$) into the unified reward for Flow-GRPO alignment:

$$\mathcal{R}_{i,g} = \omega_{\text{sv}} r_{i,g}^{\text{sv}} + \omega_{\text{map}} r_{i,g}^{\text{map}} + \omega_{\text{acc}} r_{i,g}^{\text{acc}} + \omega_{\text{sm}} r_{i,g}^{\text{sm}}. \quad (14)$$

Dataset-specific reward weights, post-training schedules, and run-time statistics are provided in the implementation details.

4 Experiments

4.1 Datasets and Evaluation Settings

We evaluate the proposed method on two widely used public benchmarks: the ETH/UCY pedestrian dataset [23, 31] and the Stanford

Drone Dataset (SDD) [33]. In all experiments, trajectories are re-sampled to 2.5 Hz. We use 8 observed frames (3.2 seconds) to predict the next 12 future frames (4.8 seconds).

4.1.1 ETH/UCY Benchmark. ETH/UCY consists of five pedestrian scenes, namely ETH, HOTEL, UNIV, ZARA1, and ZARA2, and is widely used to evaluate socially aware trajectory forecasting in crowded environments. Following the standard protocol, we adopt leave-one-out cross-validation, training on four scenes and testing on the remaining one. This benchmark is well suited to evaluating the contributions of TIG-GAT and the view-aware social reward.

4.1.2 Stanford Drone Dataset (SDD). Captured by drones over a university campus, SDD contains dense crowds in structurally complex environments. Its strong physical boundary constraints make it a suitable benchmark for evaluating the map-aware semantic reward. We precompute continuous Signed Distance Fields (SDFs) from the raw semantic scene images and report all prediction errors in pixels.

4.2 Experimental Setup

4.2.1 Baselines. We compare TIGFlow-GRPO with a representative set of trajectory forecasting baselines spanning multiple modeling paradigms. These baselines include graph-based interaction models, such as GroupNet [41] and EqMotion [42], as well as generative predictors based on diffusion or flow matching, including MID [16], SingularTrajectory [3], MoFlow [13], and the uncertainty-aware DD-MDN [19]. Since some baselines operate under different input settings, especially with respect to the availability of semantic map cues, we treat MoFlow [13] as the primary architecture-aligned baseline. This comparison highlights the contributions of TIG-GAT and Flow-GRPO beyond standard supervised flow-matching training, while the broader baseline set places our method in the context of existing trajectory forecasting paradigms.

4.2.2 Evaluation Metrics. We evaluate multimodal coverage and overall distribution quality using two groups of displacement metrics over $K = 20$ generated samples: minimum errors (ADE_{\min} , FDE_{\min}) and average errors (ADE_{avg} , FDE_{avg}). The minimum metrics compute the L_2 distance to the closest prediction, whereas the average metrics measure the mean error across all generated samples. Because the average metrics are more sensitive to low-quality or implausible samples, they provide a more informative view of

Table 2: Quantitative comparison of best-of- K ADE_{\min} and FDE_{\min} on the Stanford Drone Dataset (SDD), reported in pixels. Bold and underlined entries denote the best and second-best results, respectively.

Method	ADE	FDE
SocialGAN [17]	27.23	41.44
Y-net [28]	11.51	20.24
GroupNet [41]	9.31	16.11
MID [16]	9.73	15.32
EigenTraj [2]	8.05	13.25
LED [29]	8.49	12.67
MoFlow [13]	<u>7.63</u>	<u>12.25</u>
TIGFlow-GRPO	7.37	11.67

overall distribution quality. In addition, we report a collision rate, denoted by Col, to directly evaluate social compliance. A prediction is counted as colliding if the pairwise distance between any two agents falls below a predefined safety threshold at any future step within the evaluation horizon. Lower Col indicates better collision avoidance and complements the displacement-based metrics.

4.2.3 Implementation Details. Our framework is implemented in PyTorch and trained on a single NVIDIA RTX 3090 GPU. During pretraining, TIG-GAT uses a field-of-view angle of $\theta_{\text{FOV}} = 120^\circ$ for interaction-aware neighbor selection, and the CFM backbone is optimized with AdamW using an initial learning rate of 1×10^{-4} . During Flow-GRPO post-training, we replace deterministic ODE rollout with the proposed stochastic SDE transition and sample $G = 4$ trajectories per condition to compute group-relative advantages. All post-training experiments are conducted under the same single-GPU setting. For reproducibility, we provide the dataset-specific preprocessing protocol, including frame rate, resampling procedure, and coordinate convention, together with the reward definitions, their weights, and the post-training schedule.

4.3 Comparisons with State-of-the-Art Methods

4.3.1 Performance on ETH/UCY Benchmark. Table 1 reports the quantitative results on ETH/UCY. TIGFlow-GRPO achieves the best overall average ADE and FDE among the compared methods, reaching 0.20 and 0.31, respectively. Relative to MoFlow, the gains are consistent across all subsets and are more visible in interaction-intensive scenes such as ZARA1 and UNIV. These results indicate that TIG-GAT and Flow-GRPO improve prediction quality in socially complex scenes.

4.3.2 Performance on SDD Benchmark. To assess performance in scenes with strong physical constraints, we report the results on SDD in Table 2. Under the standard image-plane evaluation setting, TIGFlow-GRPO reduces the pixel-space ADE to 7.37 and the FDE to 11.67. Unlike ETH/UCY, SDD is strongly shaped by complex topological boundaries and non-walkable areas. The improvement over MoFlow, particularly the reduction of FDE from 12.25 to 11.67, is consistent with the role of the map-aware semantic reward in reducing boundary-crossing predictions.

Table 3: Performance degradation over extended prediction horizons on the ETH dataset, measured by ADE_{avg} and FDE_{avg} . TIGFlow-GRPO consistently outperforms the MoFlow baseline across all time steps.

ETH Time	MoFlow [13]		TIGFlow-GRPO	
	ADE_{avg}	FDE_{avg}	ADE_{avg}	FDE_{avg}
1.2s	0.33	0.52	0.29	0.46
2.4s	0.66	1.25	0.59	1.11
3.6s	1.05	2.15	0.94	1.93
4.8s	1.49	3.10	1.30	2.72

Table 4: Collision rates (%) across datasets and horizons. TIGFlow-GRPO demonstrates superior collision avoidance in most settings.

Method	Horizon	ETH	HOTEL	UNIV	ZARA1	ZARA2	SDD
MoFlow [13]	1.2s	0.55	2.83	5.72	1.14	2.63	1.92
	2.4s	3.55	4.74	13.23	3.64	8.12	12.62
	3.6s	4.92	7.81	15.92	7.94	13.26	15.85
	4.8s	5.63	9.63	19.65	11.63	16.54	19.74
TIGFlow-GRPO	1.2s	0.61	1.35	4.34	0.43	1.58	0.83
	2.4s	2.95	2.67	11.04	2.93	6.57	9.45
	3.6s	4.53	4.23	14.65	5.84	10.52	11.68
	4.8s	5.16	4.95	16.58	7.55	12.03	12.29

4.3.3 Robustness Against Error Drifting over Extended Horizons. Continuous generative forecasting models often become less reliable as the prediction horizon grows, partly because small rollout errors can accumulate over time. To assess this effect, Table 3 reports performance on ETH over extended horizons from 1.2s to 4.8s. At $t = 4.8s$, vanilla MoFlow shows a noticeable increase in FDE_{avg} , reaching 3.10, whereas TIGFlow-GRPO achieves a lower value of 2.72. This gap suggests that the proposed post-training strategy helps maintain more stable long-horizon predictions.

4.3.4 Collision Avoidance Performance. Table 4 reports Col across datasets and forecasting horizons. Compared with MoFlow, TIGFlow-GRPO achieves lower collision rates in 23 of the 24 dataset-horizon settings. The reduction is more pronounced at longer horizons, where collision risk becomes increasingly sensitive to accumulated trajectory errors. At the 4.8s horizon, Col decreases from 19.74% to 12.29% on SDD, from 9.63% to 4.95% on HOTEL, and from 16.54% to 12.03% on ZARA2. Averaged over all dataset-horizon pairs, Col drops from 8.72% to 6.45%, indicating better social compliance beyond what displacement errors alone can capture. The only minor exception appears on ETH at the 1.2s horizon, where the difference is small at 0.61% versus 0.55%. Overall, these results suggest that Flow-GRPO reduces collision-prone predictions and produces safer trajectory distributions, especially over extended horizons.

4.4 Ablation Study

To assess the contribution of each component, we conduct an ablation study on ETH. We report both minimum and average metrics to better reflect overall distribution quality. As shown in Table 5, removing any core component leads to a clear performance drop,

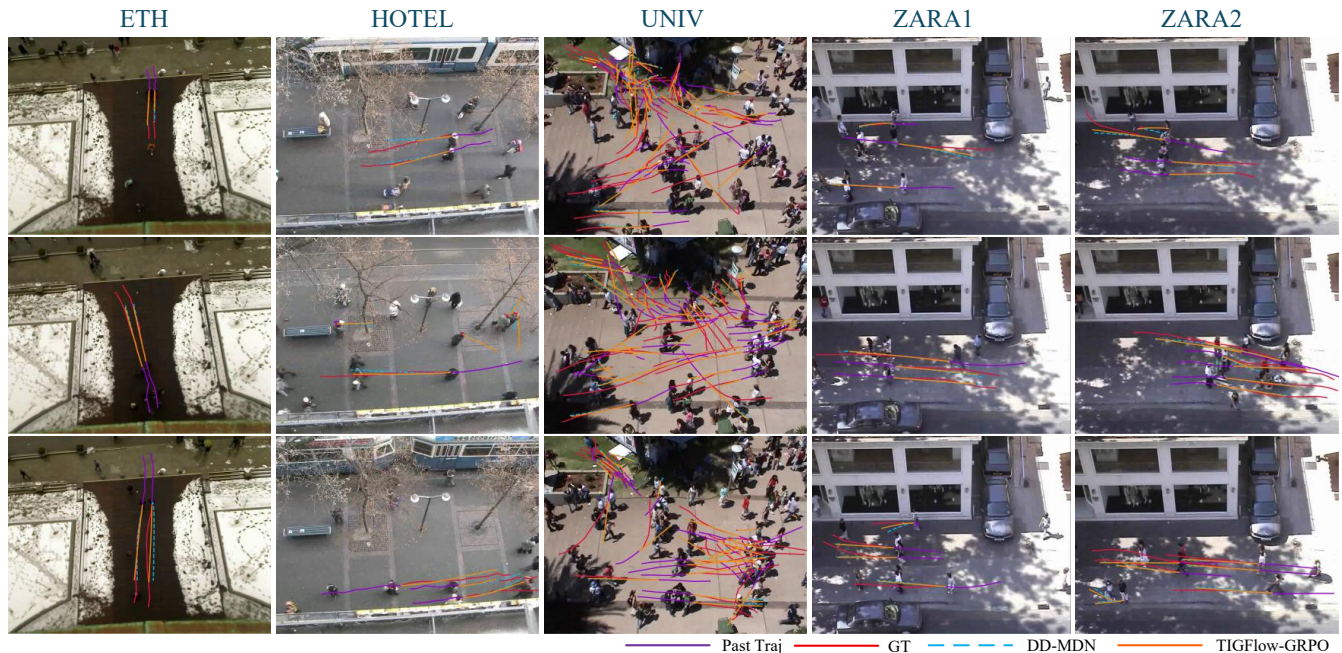


Figure 4: Qualitative results on the ETH/UCY benchmark. Compared with DD-MDN, TIGFlow-GRPO produces predictions that better follow local interaction patterns and feasible motion paths across ETH, HOTEL, UNIV, ZARA1, and ZARA2.

Table 5: Ablation study on the ETH dataset. Bold indicates the best performance. Removing any core component leads to noticeable performance degradation.

Model Variant	ETH			
	ADE _{min}	FDE _{min}	ADE _{avg}	FDE _{avg}
w/o TIG-GAT	0.404	0.593	1.494	3.103
w/o social reward	0.401	0.581	1.316	2.745
w/o map reward	0.398	0.577	1.301	2.719
w/o GRPO	0.394	0.555	1.328	2.855
Ours (Full)	0.391	0.553	1.300	2.718

with larger degradations in the average metrics, which are more sensitive to low-quality or outlier trajectories.

4.4.1 Effectiveness of TIG-GAT. When the Trajectory-Interaction-Graph Attention (TIG-GAT) module is removed, the model loses explicit local interaction modeling. As a result, although the increase in FDE_{min} is relatively modest, FDE_{avg} rises more noticeably from 2.718 to 3.103. This pattern suggests that without explicit interaction encoding, the model is more likely to generate trajectories that deviate from the local motion context and produce low-quality outliers.

4.4.2 Impact of Social and Map Rewards. We further ablate the view-aware social reward and the map-aware semantic reward individually. Removing either reward increases both the minimum

and average displacement errors. This result suggests that MLE-based pretraining alone can produce samples that appear reasonable in some cases, yet remain inconsistent with interaction patterns or scene constraints in others. Explicit social and spatial constraints are therefore important for shaping the overall trajectory distribution.

4.4.3 Necessity of GRPO Post-training. Finally, when the entire GRPO post-training stage is removed and inference reverts to deterministic ODE rollout, FDE_{avg} increases to 2.855. This degradation suggests that supervised flow-matching pretraining alone is insufficient to control low-quality samples in the predicted distribution. By contrast, GRPO post-training introduces reward-guided regularization during rollout, which suppresses outlier trajectories and improves the expected quality of the sample set. These results indicate that the contribution of GRPO extends beyond improving individual modes and also helps produce a more stable overall trajectory distribution.

4.5 Visualization

Figure 4 presents qualitative comparisons on representative cases from the five ETH/UCY scenes. In each example, purple lines denote the observed trajectories, red lines denote the ground-truth futures, yellow lines denote the predictions of DD-MDN, and orange lines denote the predictions of TIGFlow-GRPO. Compared with DD-MDN, the proposed method produces trajectory bundles that are generally tighter and better aligned with local motion structure. This difference is especially clear in crowded scenes such as UNIV, where TIGFlow-GRPO maintains multimodal diversity while avoiding the overly scattered predictions shown by DD-MDN under dense crossing flows. In ETH and HOTEL, its predictions remain

closer to the dominant walking corridor and exhibit fewer unreasonable lateral deviations. Similar behavior appears in ZARA1 and ZARA2, where TIGFlow-GRPO better follows sidewalk-like motion patterns and captures branching futures with more coherent interaction-aware samples. Overall, the visualizations show that the proposed method generates multimodal futures that are not only diverse, but also better aligned with local interactions and scene constraints.

5 Conclusion

This paper presented TIGFlow-GRPO, a two-stage framework for human trajectory forecasting in visually complex scenes. The framework combines a conditional flow-matching backbone with the TIG-GAT module to capture view-aware social interactions, and introduces an ODE-to-SDE reformulation that enables Flow-GRPO post-training in continuous trajectory space. A composite reward further incorporates social and physical constraints into the alignment process. Experiments on ETH/UCY and SDD datasets demonstrate that the proposed method improves multimodal forecasting accuracy and long-horizon robustness, while producing trajectories that better respect interaction patterns and scene constraints. Ablation results further confirm that both TIG-GAT and reward-guided post-training contribute to these gains. In future work, we plan to extend the framework with richer visual inputs and VLM-based scene reasoning for more general motion prediction in intelligent multimedia systems.

Acknowledgments

To Robert, for the bagels and explaining CMYK and color spaces.

References

- [1] Michael Albergo, Nicholas M Boffi, and Eric Vanden-Eijnden. 2025. Stochastic interpolants: A unifying framework for flows and diffusions. *Journal of Machine Learning Research* 26, 209 (2025), 1–80.
- [2] Inhwan Bae, Jean Oh, and Hae-Gon Jeon. 2023. Eigentrjectory: Low-rank descriptors for multi-modal trajectory forecasting. In *Proceedings of the IEEE/CVF International Conference on Computer Vision*. 10017–10029.
- [3] Inhwan Bae, Young-Jae Park, and Hae-Gon Jeon. 2024. Singulartrajectory: Universal trajectory predictor using diffusion model. In *Proceedings of the IEEE/CVF Conference on Computer Vision and Pattern Recognition*. 17890–17901.
- [4] Mohammadhossein Bahari, Saeed Saadatnejad, Amirhossein Askari Farsangi, Seyed-Mohsen Moosavi-Dezfooli, and Alexandre Alahi. 2025. Certified human trajectory prediction. In *Proceedings of the Computer Vision and Pattern Recognition Conference*. 12301–12311.
- [5] Tim Brooks, Bill Peebles, Connor Holmes, Will DePue, Yufei Guo, Leo Jing, David Schnurr, Joe Taylor, Troy Luhman, Eric Luhman, et al. 2024. Video generation models as world simulators. *OpenAI Blog* 1, 8 (2024), 1.
- [6] Prafulla Dhariwal and Alexander Nichol. 2021. Diffusion models beat gans on image synthesis. *Advances in neural information processing systems* 34 (2021), 8780–8794.
- [7] Carles Domingo-Enrich, Michal Drozdal, Brian Karrer, and Ricky TQ Chen. 2024. Adjoint matching: Fine-tuning flow and diffusion generative models with memoryless stochastic optimal control. *arXiv preprint arXiv:2409.08861* (2024).
- [8] Zhiwei Dong, Ran Ding, Wei Li, Peng Zhang, Guobin Tang, and Jia Guo. 2025. Leveraging sd map to augment hd map-based trajectory prediction. In *Proceedings of the Computer Vision and Pattern Recognition Conference*. 17219–17228.
- [9] Patrick Esser, Sumith Kulal, Andreas Blattmann, Rahim Entezari, Jonas Müller, Harry Saini, Yam Levi, Dominik Lorenz, Axel Sauer, Frederic Boesel, et al. 2024. Scaling rectified flow transformers for high-resolution image synthesis. In *Forty-first international conference on machine learning*.
- [10] Jiajun Fan, Shuaike Shen, Chaoran Cheng, Yuxin Chen, Chumeng Liang, and Ge Liu. 2025. Online reward-weighted fine-tuning of flow matching with wasserstein regularization. In *The Thirteenth International Conference on Learning Representations*.
- [11] Ying Fan, Olivia Watkins, Yuqing Du, Hao Liu, Moonkyung Ryu, Craig Boutilier, Pieter Abbeel, Mohammad Ghavamzadeh, Kangwook Lee, and Kimin Lee. 2023. Reinforcement learning for fine-tuning text-to-image diffusion models. In *Thirty-seventh Conference on Neural Information Processing Systems (NeurIPS) 2023*. Neural Information Processing Systems Foundation.
- [12] Zilin Fang, David Hsu, Gim Hee Lee, and Gim Hee Lee. 2025. Neuralized Markov Random Field for Interaction-Aware Stochastic Human Trajectory Prediction.. In *ICLR*.
- [13] Yuxiang Fu, Qi Yan, Lele Wang, Ke Li, and Renjie Liao. 2025. Moflow: One-step flow matching for human trajectory forecasting via implicit maximum likelihood estimation based distillation. In *Proceedings of the Computer Vision and Pattern Recognition Conference*. 17282–17293.
- [14] Tianci Gao, Yuzhen Zhang, Hang Guo, and Pei Lv. 2025. SocialMP: Learning Social Aware Motion Patterns via Additive Fusion for Pedestrian Trajectory Prediction. In *Proceedings of the Thirty-Fourth International Joint Conference on Artificial Intelligence*. 90–98.
- [15] Itai Gat, Tal Remez, Neta Shaul, Felix Kreuk, Ricky TQ Chen, Gabriel Synnaeve, Yossi Adi, and Yaron Lipman. 2024. Discrete flow matching. *Advances in Neural Information Processing Systems* 37 (2024), 133345–133385.
- [16] Tianpei Gu, Guangyi Chen, Junlong Li, Chunze Lin, Yongming Rao, Jie Zhou, and Jiwen Lu. 2022. Stochastic trajectory prediction via motion indeterminacy diffusion. In *Proceedings of the IEEE/CVF conference on computer vision and pattern recognition*. 17113–17122.
- [17] Agrim Gupta, Justin Johnson, Li Fei-Fei, Silvio Savarese, and Alexandre Alahi. 2018. Social gan: Socially acceptable trajectories with generative adversarial networks. In *Proceedings of the IEEE conference on computer vision and pattern recognition*. 2255–2264.
- [18] Manuel Hetzel, Hannes Reichert, Konrad Doll, and Bernhard Sick. 2024. Reliable probabilistic human trajectory prediction for autonomous applications. In *European Conference on Computer Vision*. Springer, 135–152.
- [19] Manuel Hetzel, Kerim Turacan, Hannes Reichert, Konrad Doll, and Bernhard Sick. 2026. DD-MDN: Human Trajectory Forecasting with Diffusion-Based Dual Mixture Density Networks and Uncertainty Self-Calibration. *arXiv preprint arXiv:2602.11214* (2026).
- [20] Jonathan Ho, Ajay Jain, and Pieter Abbeel. 2020. Denoising diffusion probabilistic models. *Advances in neural information processing systems* 33 (2020), 6840–6851.
- [21] Jaewoo Jeong, Seohee Lee, Daehee Park, Giwon Lee, and Kuk-Jin Yoon. 2025. Multi-modal knowledge distillation-based human trajectory forecasting. In *Proceedings of the Computer Vision and Pattern Recognition Conference*. 24222–24233.
- [22] Chiyu Jiang, Andre Cornman, Cheolho Park, Benjamin Sapp, Yin Zhou, Dragomir Anguelov, et al. 2023. Motiandiffuser: Controllable multi-agent motion prediction using diffusion. In *Proceedings of the IEEE/CVF conference on computer vision and pattern recognition*. 9644–9653.
- [23] Alon Lerner, Yiorgos Chrysanthou, and Dani Lischinski. 2007. Crowds by example. In *Computer graphics forum*, Vol. 26. Wiley Online Library, 655–664.
- [24] Yaron Lipman, Ricky TQ Chen, Heli Ben-Hamu, Maximilian Nickel, and Matt Le. 2022. Flow matching for generative modeling. *arXiv preprint arXiv:2210.02747* (2022).
- [25] Jie Liu, Gongye Liu, Jiajun Liang, Yangguang Li, Jiaheng Liu, Xintao Wang, Pengfei Wan, Di Zhang, and Wanli Ouyang. 2025. Flow-grpo: Training flow matching models via online rl. *arXiv preprint arXiv:2505.05470* (2025).
- [26] Jiayi Liu, Jiaming Zhou, Ke Ye, Kun-Yu Lin, Allan Wang, and Junwei Liang. 2025. EgoTraj-Bench: Towards Robust Trajectory Prediction Under Ego-view Noisy Observations. *arXiv preprint arXiv:2510.00405* (2025).
- [27] Xingchao Liu, Chengyue Gong, and Qiang Liu. 2022. Flow straight and fast: Learning to generate and transfer data with rectified flow. *arXiv preprint arXiv:2209.03003* (2022).
- [28] Karttikeya Mangalam, Yang An, Harshayu Girase, and Jitendra Malik. 2021. From goals, waypoints & paths to long term human trajectory forecasting. In *Proceedings of the IEEE/CVF international conference on computer vision*. 15233–15242.
- [29] Weibo Mao, Chenxin Xu, Qi Zhu, Siheng Chen, and Yanfeng Wang. 2023. Leapfrog diffusion model for stochastic trajectory prediction. In *Proceedings of the IEEE/CVF conference on computer vision and pattern recognition*. 5517–5526.
- [30] Long Ouyang, Jeffrey Wu, Xu Jiang, Diogo Almeida, Carroll Wainwright, Pamela Mishkin, Chong Zhang, Sandhini Agarwal, Katarina Slama, Alex Ray, et al. 2022. Training language models to follow instructions with human feedback. *Advances in neural information processing systems* 35 (2022), 27730–27744.
- [31] Stefano Pellegrini, Andreas Ess, Konrad Schindler, and Luc Van Gool. 2009. You'll never walk alone: Modeling social behavior for multi-target tracking. In *2009 IEEE 12th international conference on computer vision*. IEEE, 261–268.
- [32] Adam Polyak, Amit Zohar, Andrew Brown, Andros Tjandra, Animesh Sinha, Ann Lee, Apoorv Vyas, Bowen Shi, Chih-Yao Ma, and Chuang. 2024. Movie gen: A cast of media foundation models. *arXiv preprint arXiv:2410.13720* (2024).
- [33] Alexandre Robicquet, Amir Sadeghian, Alexandre Alahi, and Silvio Savarese. 2016. Learning social etiquette: Human trajectory understanding in crowded scenes. In *European conference on computer vision*. Springer, 549–565.
- [34] Tim Salzmann, Boris Ivanovic, Punarjay Chakravarty, and Marco Pavone. 2020. Trajectron++: Dynamically-feasible trajectory forecasting with heterogeneous data. In *European conference on computer vision*. Springer, 683–700.

- [35] Zhihong Shao, Peiyi Wang, Qihao Zhu, Runxin Xu, Junxiao Song, Xiao Bi, Haowei Zhang, Mingchuan Zhang, YK Li, Yang Wu, et al. 2024. Deepseekmath: Pushing the limits of mathematical reasoning in open language models. *arXiv preprint arXiv:2402.03300* (2024).
- [36] Yang Song, Jascha Sohl-Dickstein, Diederik P Kingma, Abhishek Kumar, Stefano Ermon, and Ben Poole. 2020. Score-based generative modeling through stochastic differential equations. *arXiv preprint arXiv:2011.13456* (2020).
- [37] Nisan Stiennon, Long Ouyang, Jeffrey Wu, Daniel Ziegler, Ryan Lowe, Chelsea Voss, Alec Radford, Dario Amodei, and Paul F Christiano. 2020. Learning to summarize with human feedback. *Advances in neural information processing systems* 33 (2020), 3008–3021.
- [38] Xiaohui Sun, Ruitong Xiao, Jianye Mo, Bowen Wu, Qun Yu, and Baoxun Wang. 2025. F5r-tts: Improving flow-matching based text-to-speech with group relative policy optimization. *arXiv preprint arXiv:2504.02407* (2025).
- [39] Ashish Vaswani, Noam Shazeer, Niki Parmar, Jakob Uszkoreit, Llion Jones, Aidan N Gomez, Łukasz Kaiser, and Illia Polosukhin. 2017. Attention is all you need. *Advances in neural information processing systems* 30 (2017).
- [40] Liwen Xiao, Zhiyu Pan, Zhicheng Wang, Zhiguo Cao, and Wei Li. 2025. SRefiner: Soft-Braid Attention for Multi-Agent Trajectory Refinement. In *Proceedings of the IEEE/CVF International Conference on Computer Vision*. 960–969.
- [41] Chenxin Xu, Maosen Li, Zhenyang Ni, Ya Zhang, and Siheng Chen. 2022. Groupnet: Multiscale hypergraph neural networks for trajectory prediction with relational reasoning. In *Proceedings of the IEEE/CVF conference on computer vision and pattern recognition*. 6498–6507.
- [42] Chenxin Xu, Robby T Tan, Yuhong Tan, Siheng Chen, Yu Guang Wang, Xinchao Wang, and Yanfeng Wang. 2023. Eqmotion: Equivariant multi-agent motion prediction with invariant interaction reasoning. In *Proceedings of the IEEE/CVF conference on computer vision and pattern recognition*. 1410–1420.
- [43] Pei Xu, Jean-Bernard Hayet, and Ioannis Karamouzas. 2022. Socialvae: Human trajectory prediction using timewise latents. In *European Conference on Computer Vision*. Springer, 511–528.
- [44] Yi Xu, Lichen Wang, Yizhou Wang, and Yun Fu. 2022. Adaptive trajectory prediction via transferable gnn. In *Proceedings of the IEEE/CVF conference on computer vision and pattern recognition*. 6520–6531.
- [45] Shuchen Xue, Chongjian Ge, Shilong Zhang, Yichen Li, and Zhi-Ming Ma. 2025. Advantage weighted matching: Aligning rl with pretraining in diffusion models. *arXiv preprint arXiv:2509.25050* (2025).
- [46] Junjie Zheng, Chunbo Hao, Guobin Ma, Xiaoyu Zhang, Gongyu Chen, Chaofan Ding, Zihao Chen, and Lei Xie. 2025. YingMusic-Singer: Zero-shot Singing Voice Synthesis and Editing with Annotation-free Melody Guidance. *arXiv preprint arXiv:2512.04779* (2025).